Electronic Supplementary Material (ESI) for CrystEngComm.
This journal is © The Royal Society of Chemistry 2016

Supporting Information

# Controlling Interpenetration for Tuning Porosity and Luminescence Properties on Flexible MOFs Based on Biphenyl-4,4′-dicarboxylic acid

Belén Fernández,[a] Garikoitz Beobide,[b] Ignacio Sánchez,[a] Francisco Carrasco,[a] José M. Seco,[c] Antonio J. Calahorro,[a] Javier Cepeda,[c,d,*] and Antonio Rodríguez-Diéguez[a,*]

[a] Departamento de Química Inorgánica, Universidad de Granada, 18071, Granada, Spain. [b] Departamento de Química Inorgánica, Facultad de Ciencia y Tecnología, Universidad del País Vasco/Euskal Herriko Unibertsitatea, UPV/EHU, Apdo. 644, 48080, Bilbao, Spain. [c] Departamento de Química Aplicada, and [d] Departamento de Ciencia y Tecnología de Polímeros, Facultad de Química, Universidad del País Vasco/Euskal Herriko Unibertsitatea, UPV/EHU, 20018, San Sebastián, Spain.

FTIR spectra ($cm^{-1}$, KBr pellet) for compounds **1**–**4**:

$\{[Cd_3(\mu_4\text{-bpdc})_3(H_2O)_2]\cdot DMF\}_n$ (**1**): 3185 (m), 1610 (m), 1600 (sh), 1580 (s), 1520 (s), 1395 (s), 1180 (w), 1030 (w), 1000 (w), 850 (w), 820 (w), 765 (m), 690 (w).

$\{[Zn_3(\mu_4\text{-bpdc})_3(\mu\text{-bpdb})]\cdot 5DMF\}_n$ (**2**):3250 (m), 1605 (m), 1595(s), 1565(s), 1420(s), 1027(w), 851(w), 814(w), 780(s), 600(w).

$\{[Zn_2(\mu 4\text{-bpdc})_2(\mu\text{-bpdb})]\cdot 7DMF\}_n$ (**3**): 3250 (m), 1620 (s), 1580 (m), 1550 (s), 1500 (s), 1365 (s), 1150 (w), 1025 (w), 860 (w), 820 (w), 750 (m), 650 (w).

$\{[Zn_4(\mu_4\text{-bpdc})_3(DMF)(\mu_4\text{-}O)(H_2O)]\cdot 7DMF\cdot 3H_2O\}_n$ (**4**): 3195 (m), 1605 (m), 1577 (s), 1525 (s), 1395 (s), 1180 (w), 1025 (w), 1000 (w), 850 (w), 815 (w), 765 (m), 685 (w).

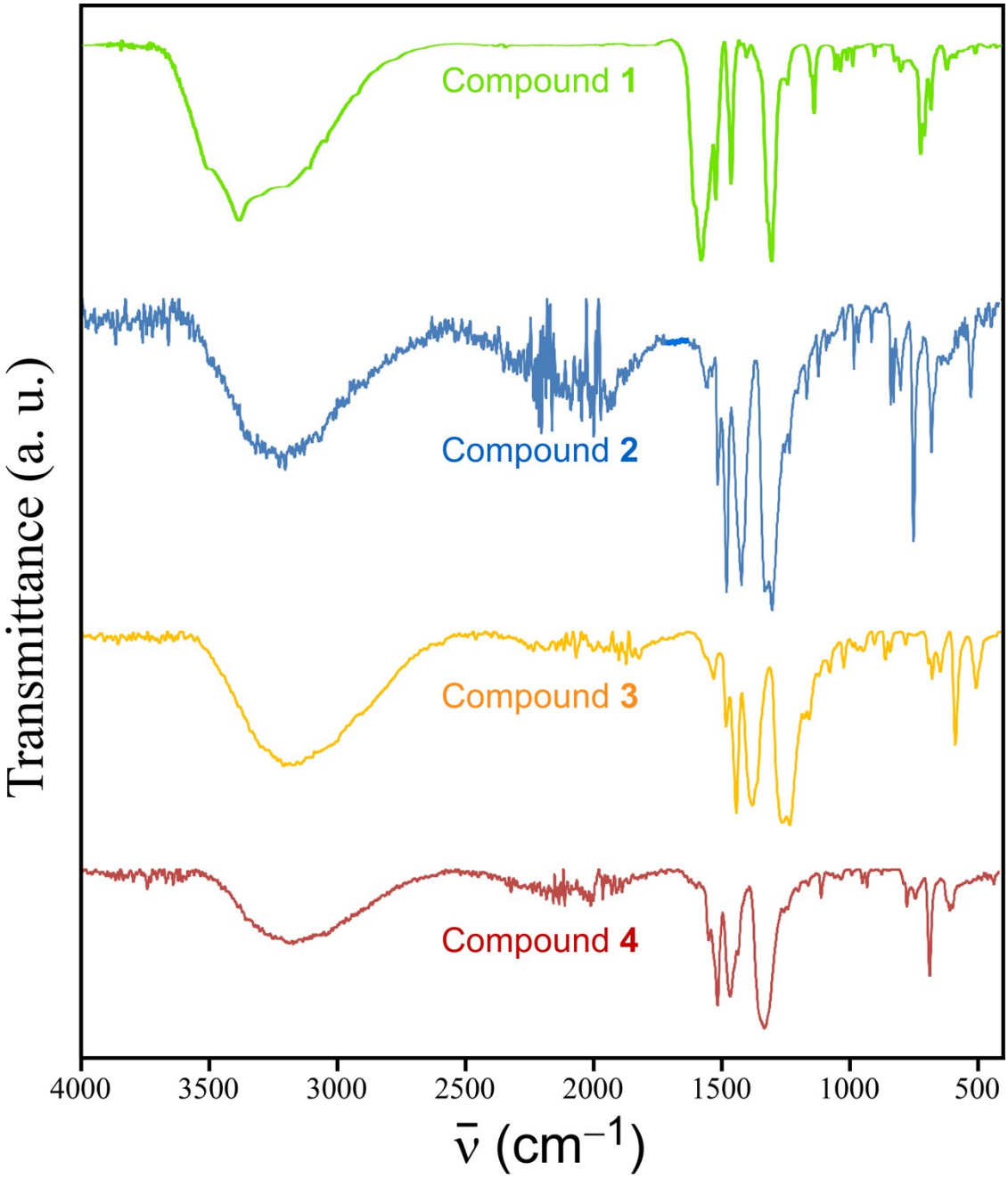


**Figure S1.** FTIR spectra of all compounds.

Pattern-matching analyses for compounds **1**–**4**:

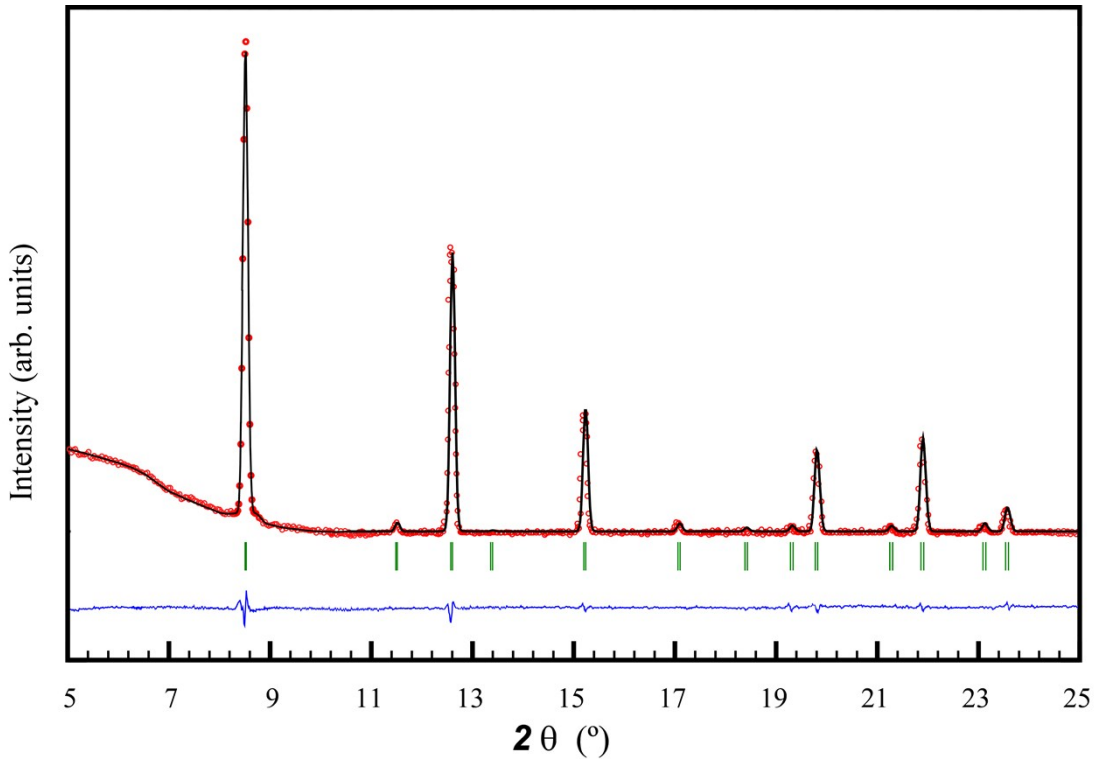


**Figure S2.** Pattern-matching analysis of compound **1**.

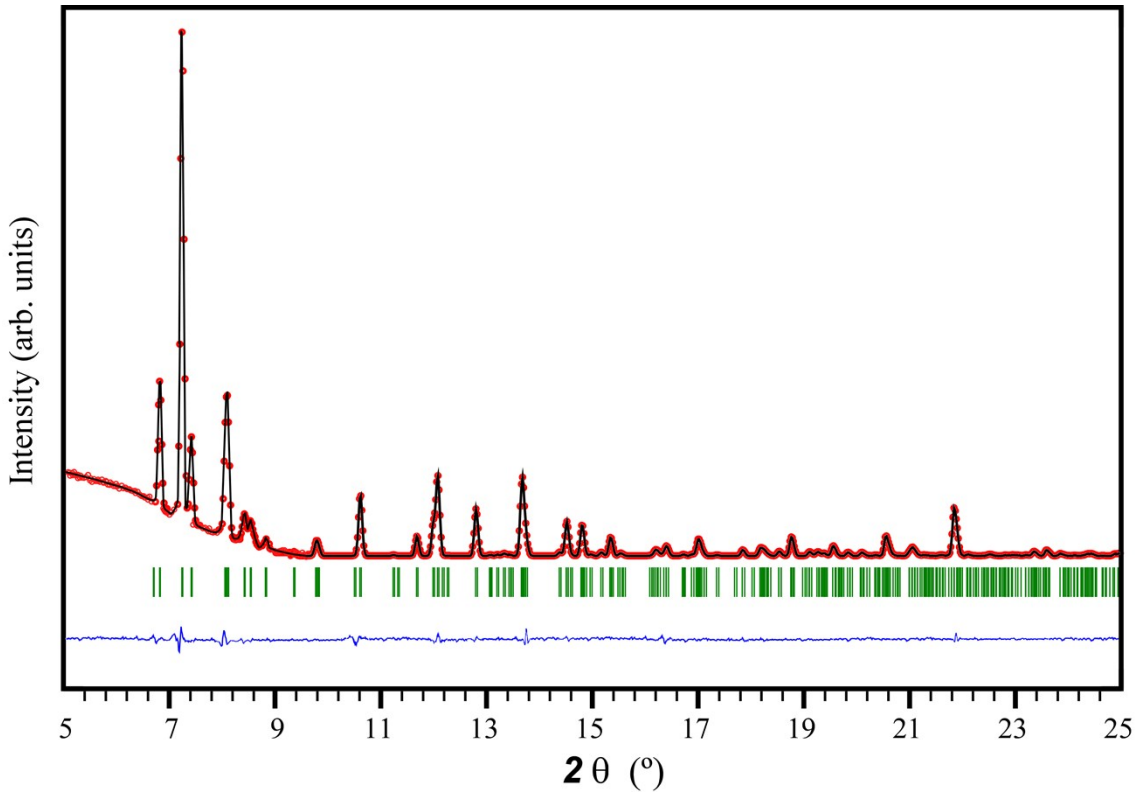


**Figure S3.** Pattern-matching analysis of compound **2**.

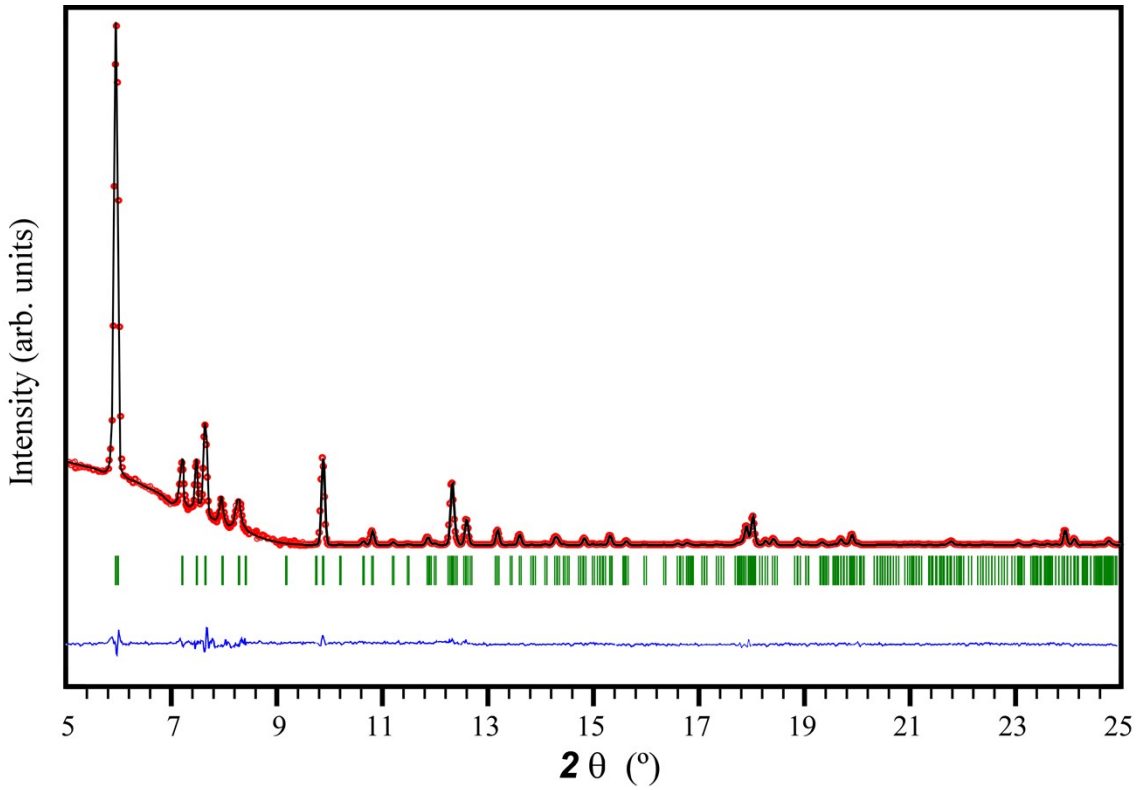


**Figure S4.** Pattern-matching analysis of compound **3**.

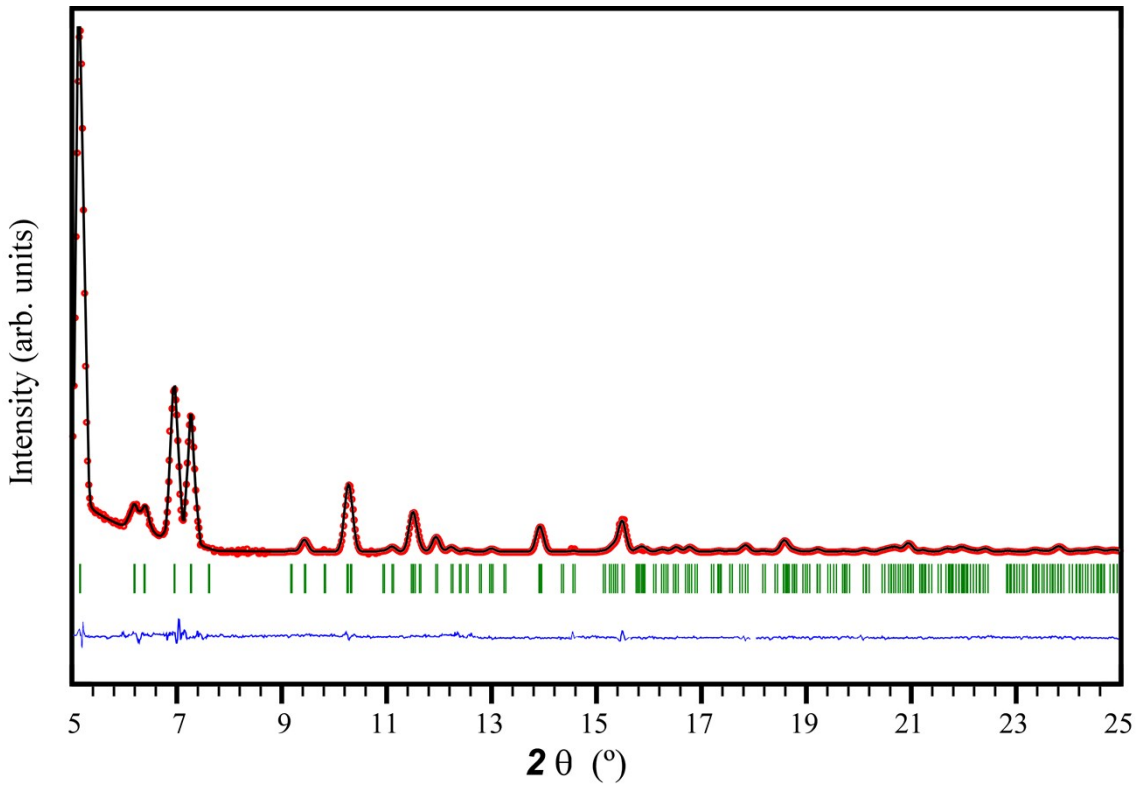


**Figure S5.** Pattern-matching analysis of compound **4**.

Additional figures of crystal structures of compounds **1**–**4**:

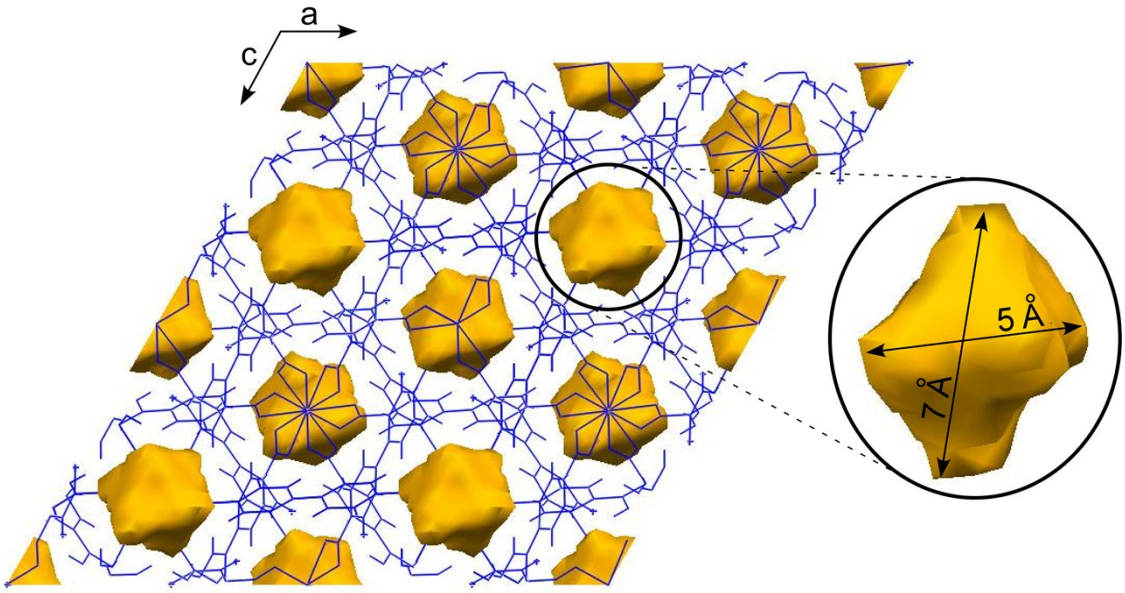


**Figure S6.** Crystal packing of layers of compound **1** along b axis showing the isolated voids.

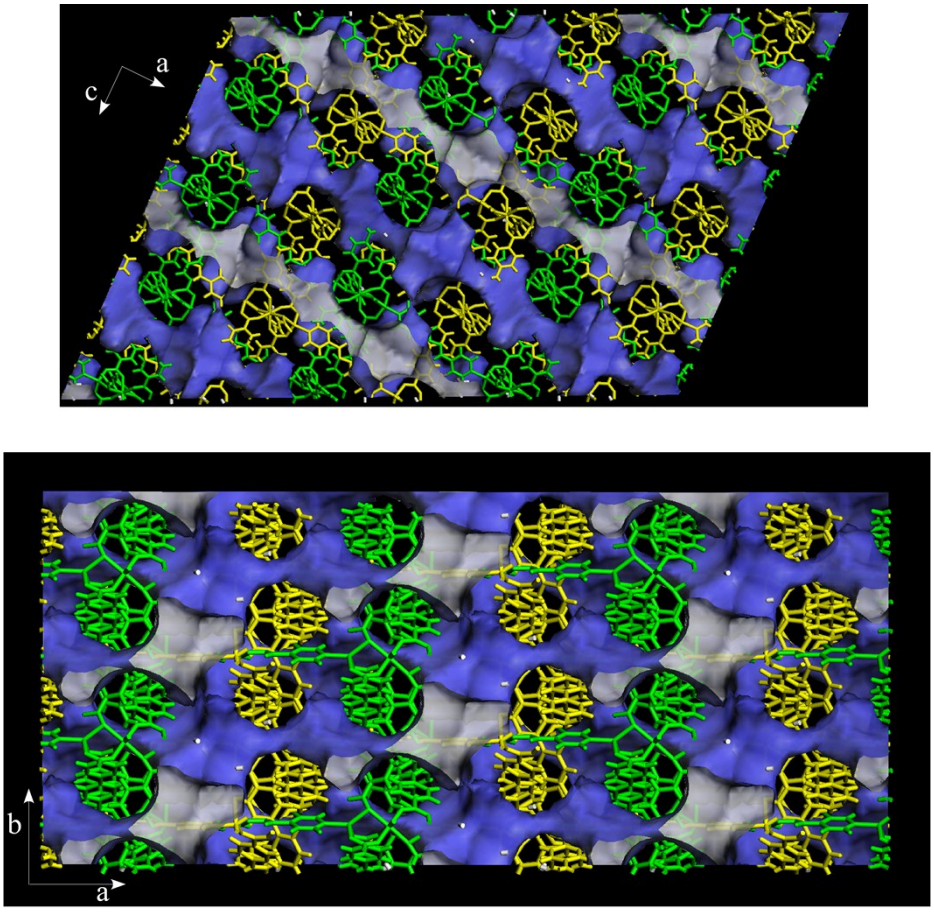


**Figure S7.** View of the accessible surface for a $N_2$ probe (3.681 Å) in the doubly interpenetrated structure of compound **3** along [001] and [010] directions.

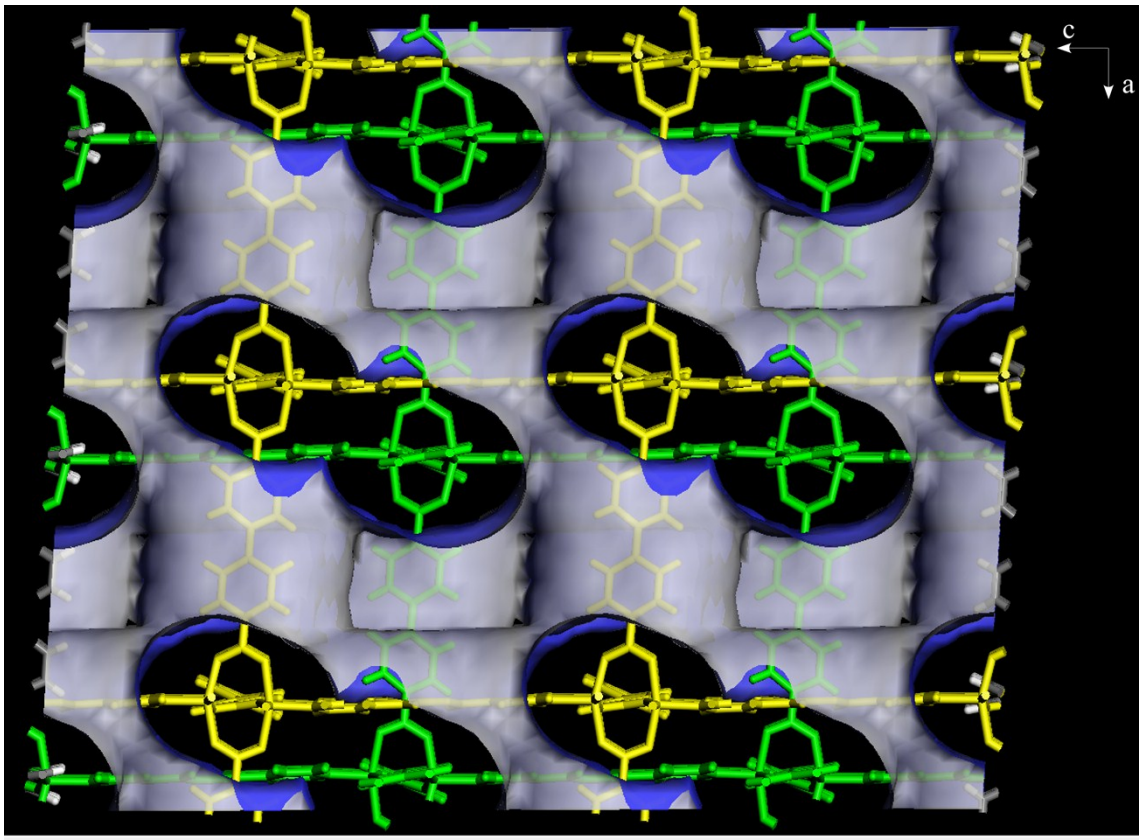


**Figure S8.** A representation of the accessible surface for a $N_2$ probe (3.681 Å) in the doubly interpenetrated structure of compound **3** along [010] direction.

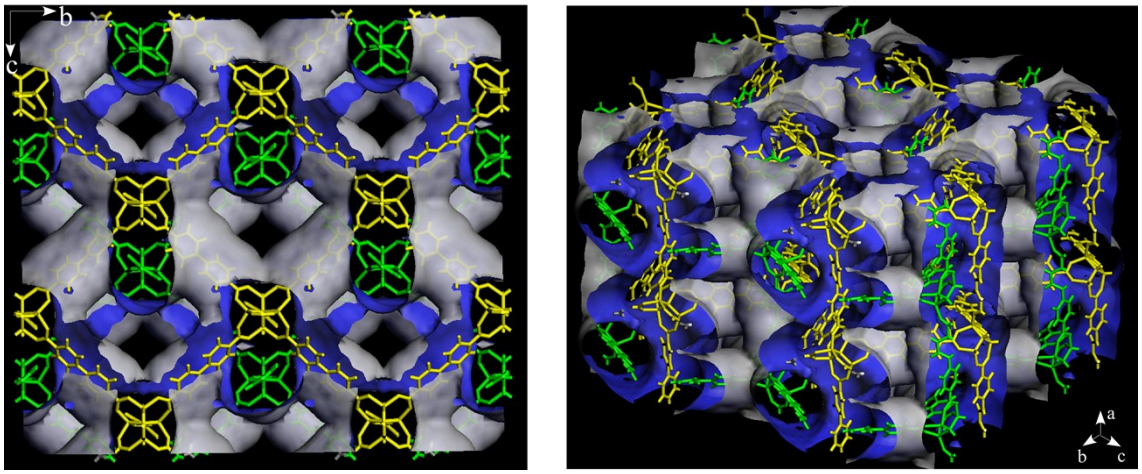


**Figure S9.** A representation of the accessible surface for a $N_2$ probe (3.681 Å) in the doubly interpenetrated structure of compound **4** along [100] and [111] directions.

ThermoGravimetric/Differential Thermal Analyses of compounds **1**–**4**:

**Table S1.** Elemental analysis and TG/DTA curves of compound **1**.

| $\{[Cd_3(\mu_4\text{-bpdc})_3(H_2O)_2]\cdot DMF\}_n$ | | |
|---|---|---|
| **$C_{45}H_{35}Cd_3NO_{15}$** | | |
| **Ti–Tf** | **ΣΔm(%)** | **$\Sigma\Delta m(\%)_{teor}$** |
| 30–220 | 10.1 | 9.4 ($-2H_2O$+1DMF) |
| 290–400 | 66.7 | 67.0 (CdO) |

**Elemental analysis**

Anal. Calc.: C, 46.31; H, 3.02; Cd, 28.90; N, 1.20%. Found: C, 46.07; H, 3.25; Cd, 29.02; N, 1.38%.

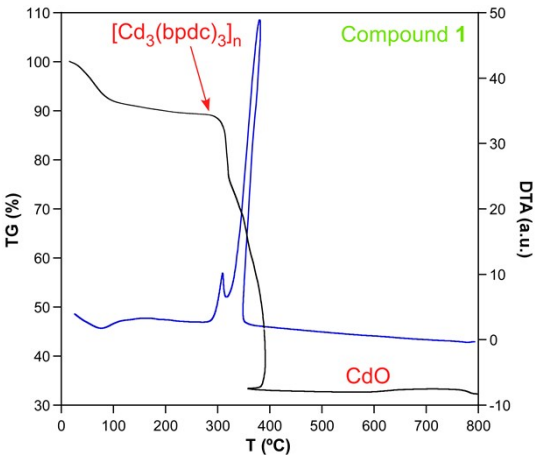


**Table S2.** Elemental analysis and TG/DTA curves of compound **2**.

| $\{[Zn_3(\mu_4\text{-bpdc})_3(\mu\text{-bpdb})]\cdot 5DMF\}_n$ | | |
|---|---|---|
| **$C_{69}H_{69}N_9O_{17}Zn_3$** | | |
| **Ti–Tf** | **ΣΔm(%)** | **$\Sigma\Delta m(\%)_{teor}$** |
| 30–150 | 25.1 | 24.5 (–5 DMF) |
| 285–480 | 83.5 | 83.6 (ZnO) |

**Elemental analysis**

Anal. Calc.: C, 55.53; H, 4.66; N, 8.45; Zn, 13.14%. Found: C, 55.35; H, 4.43; N, 8.59; Zn, 13.35%.

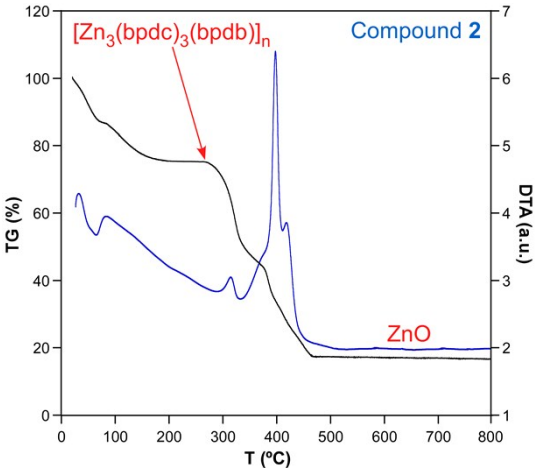

**Table S3.** Elemental analysis and TG/DTA curves of compound **3**.

$\{[Zn_2(\mu_4\text{-bpdc})_2(\mu\text{-bpdb})]\cdot 7DMF\}_n$

**$C_{61}H_{75}N_{11}O_{15}Zn_2$**

| **Ti–Tf** | **$\Sigma\Delta m(\%)$** | **$\Sigma\Delta m(\%)_{teor}$** |
|---|---|---|
| 30–150 | 37.7 | 38.3 (–7DMF) |
| 285–480 | 88.5 | 87.8 (ZnO) |

**Elemental analysis**

Anal. Calc.: C, 54.96; H, 5.67; N, 11.56; Zn, 9.81%. Found: C, 55.08; H, 5.55; N, 11.82; Zn, 9.76%.

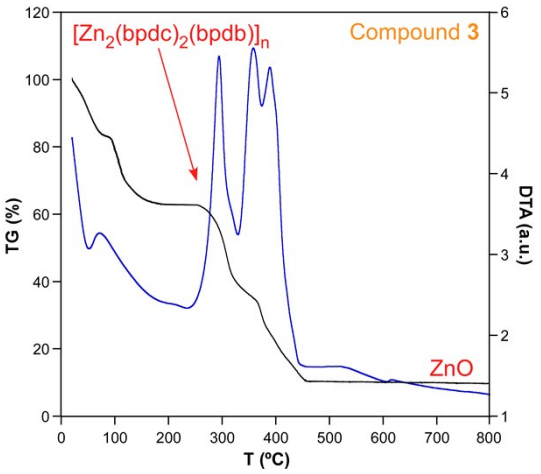


**Table S4.** Elemental analysis and TG/DTA curves of compound **4**.

$\{[Zn_4(\mu_4\text{-bpdc})_3(DMF)(\mu_4\text{-}O)(H_2O)]\cdot 7DMF\cdot 3H_2O\}_n$

**$C_{66}H_{88}N_8O_{25}Zn_4$**

| **Ti–Tf** | **$\Sigma\Delta m(\%)$** | **$\Sigma\Delta m(\%)_{teor}$** |
|---|---|---|
| 30–150 | 34.9 | 34.2 (–7DMF+3$H_2O$) |
| 30–150 | 40.6 | 39.7 (–8DMF+4$H_2O$) |
| 285–480 | 19.9 | 20.3 (ZnO) |

**Elemental analysis**

Anal. Calc.: C, 47.90; H, 5.36; N, 6.77; Zn, 15.80%. Found: C, 47.98; H, 5.25; N, 6.82; Zn, 15.56%.

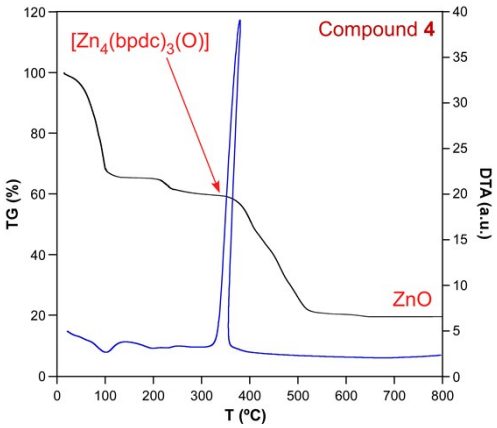

Brief description on accessible surface area and pore size distributions calculated by the Sarkisov and Harrison methodology employed (Reference 31 in the article):

Calculation of the accessible surface area is performed through a Monte Carlo procedure in which the atoms of the adsorbent are sequentially considered, defining for each a sphere of a diameter $\sigma = \sigma_a + \sigma_p$, where $\sigma_a$ is the diameter of the adsorbent atom and $\sigma_p$ is the diameter of the probe particle. Hereafter, points are randomly generated on the surface of the sphere. A probe particle is placed in each generated point and tested for the overlaps with the other atoms of the structure. The accessible surface area of the atom under consideration is obtained by subtracting from the total sphere area the fraction corresponding to points that imply an overlap between the probe particle and other atoms of the structure. The accessible area of the adsorbent is calculated summing the individual accessible areas of the adsorbent atoms. For a more accurate correlation with BET area the calculation accessible surface is based on the distance corresponding to the potential minimum according to the Lennard-Jones equation. The parameters describing the adsorbent atoms have been obtained from the universal force field (UFF), while as molecular probe a single point DREIDING model of $N_2$ (3.314 Å) was selected.

Pore size distributions (PSD) are estimated also according to a Monte Carlo procedure. The simulation cell is divided in small bins in which a test point **a** is randomly placed in the simulation cell and tested for the overlaps with the adsorbent atoms at a distance defined on the basis of the universal force field parameters. No overlapping points are employed in successive Monte Carlo rounds, where an incremental size of the particle sited in point **a** probes the largest sphere that does not overlap with the atoms of the adsorbent. Amount of bins decrease with the increase of the probe size and the normalized bin distribution depicts a curve with decreasing steps that limit and define the pores of the structure, resembling a cumulative pore volume function $V_p(r)$, the

volume fraction that can be covered by spheres of radius $r$ or smaller. The derivative $-\mathrm{d}V_\mathrm{p}(r)/\mathrm{d}r$ yields the pore size distribution.